Supporting Information

Aqueous rechargeable ammonium ion battery based on the MoS_2/MXene with ball-flower morphology as anode and $NH_4V_4O_{10}$ with layered structure as cathode

Xue Bai[a], Jiahan Yang[a], Fengying Zhang[a], Zhuwu Jiang[a]*, Fengyi Sun[a], Chuntao Pan[a], Hongcheng Di[a], Shining Ru[a], Dongqi Liao[a], Hongyu Zhang[a]*

a. College of Ecological Environment and Urban Construction, Fujian University of Technology, Xuefu South Road, No.33, University New District, Fuzhou 350108, Fujian, P.R. China

Supporting Information consists of six figure and one Table over nine pages, which are Fig. S1 about the N_2 adsorption-desorption isotherms, Fig. S2 the SEM images of both eelctrodes after cycling, Fig. S3 about the CV curves of both electrodes, Fig. S4 about the SEM images of three samples, Fig. S5 about electrolyte screening test, Fig. S6 about the GITT tests of three electrodes, Fig. S7 about the N1s of XPS pattern of electrodes at different states, Fig. S8 about the CV at 2 mV of full battery and Table S1 The performance comparison of different electrode.

*Corresponding authors.
E-mail addresses: jiangzhuwu@126.com; zhybattery@fjut.edu.cn

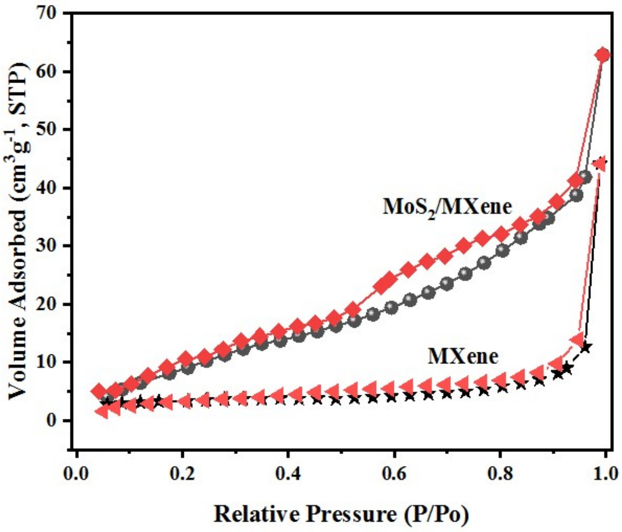

Fig. S1. The N_2 adsorption-desorption isotherms of MoS_2 and MoS_2/MXene.

Fig. S1 shows the N_2 adsorption-desorption isotherms of MoS_2 and MoS_2/MXene, of which the corresponding specific surface areas are 11.3 and 45 m²/g, respectively. This result further demonstrates that MoS_2/MXene shows more excellent electrochemical performance.

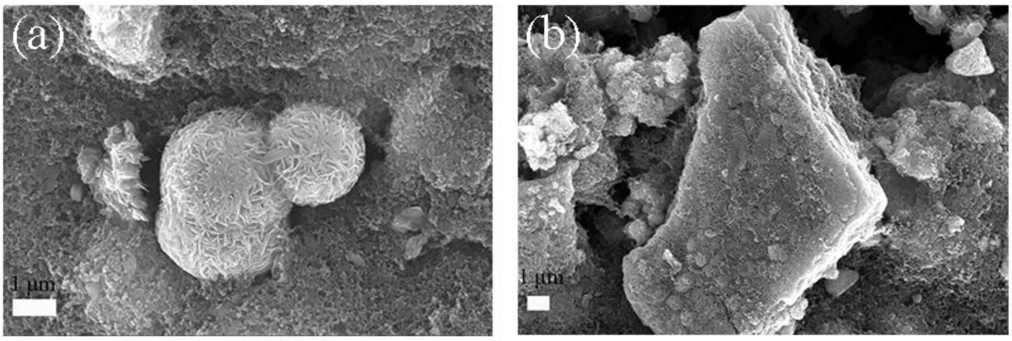

Fig. S2. The SEM images of MoS_2 and MoS_2/MXene anodes after cycling.

Fig. S2 shows the SEM images of MoS_2 and MoS_2/MXene anodes after 100 cycles at current density of 100 mA g^{-1}. It can be found both of electrodes maintained the ball-flower morphology. And the composite maintains a better stable structure.

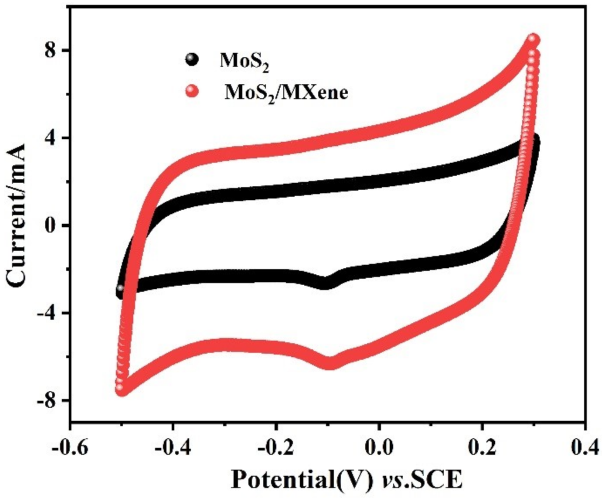

Fig. S3. The CV curves of MoS_2 and MoS_2/MXene.

Fig. S3 shows the CV comparison of MoS_2 and MoS_2/MXene, which exhibits the pseudocapacitance behavior. It is clearly found that MoS_2/MXene displays better electrochemical properties than single MoS_2 in aqueous ammonium ion battery.

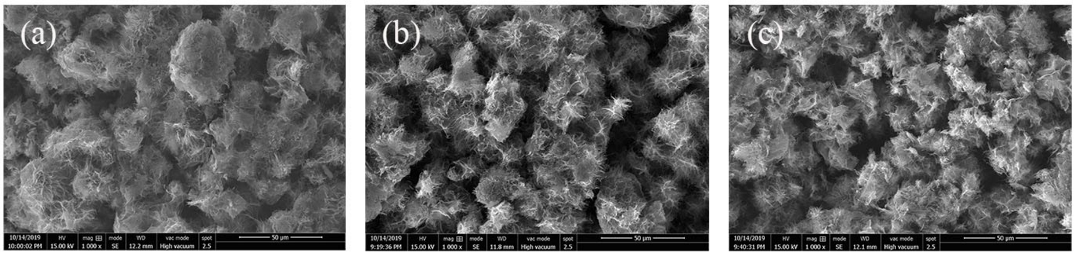

Fig. S4. SEM images of $NH_4V_4O_{10}$ samples prepared at 140 °C (a), 160 °C (b), and 180 °C (c)

In the small magnification electron microscopy, we can clearly find that the single nanowire flower of $NH_4V_4O_{10}$ sample become smaller with the increasing of preparation temperature.

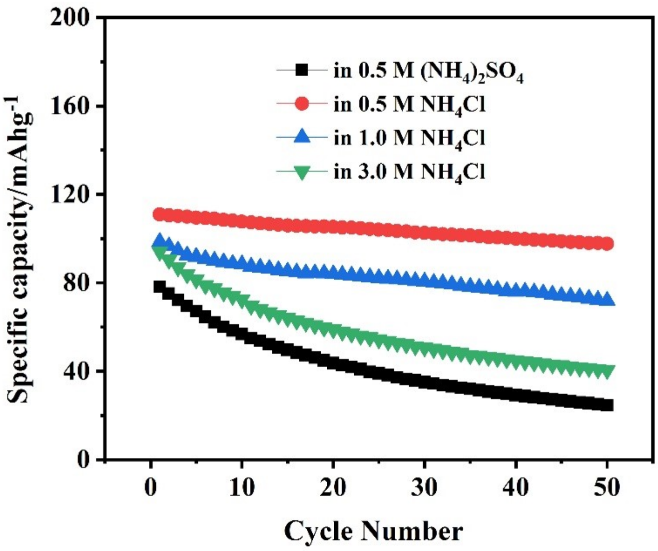

Fig. S5. The cycle performance of electrodes in different electrolytes.

It is clearly observed that the $NH_4V_4O_{10}$ electrode in 0.5 mol dm^{-3} NH_4Cl electrolyte exhibits the best cycle performance than other electrolytes.

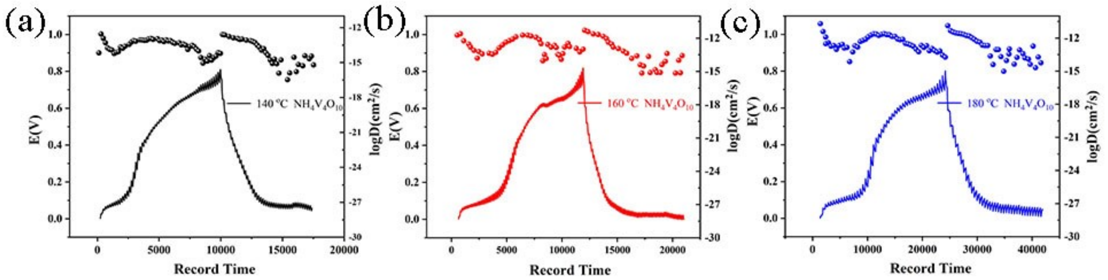

Fig. S6. The GITT tests of three electrodes

The GITT measurements of three electrodes are also tested in Fig. S6. It can be found that the average D value of electrode at 180 ^{o}C is larger than that of other electrodes, which demonstrates that the $NH_4V_4O_{10}$ electrode at 180 ^{o}C shows the fast ammonium ion diffusion kinetics and it can exhibit excellent electrochemical properties.

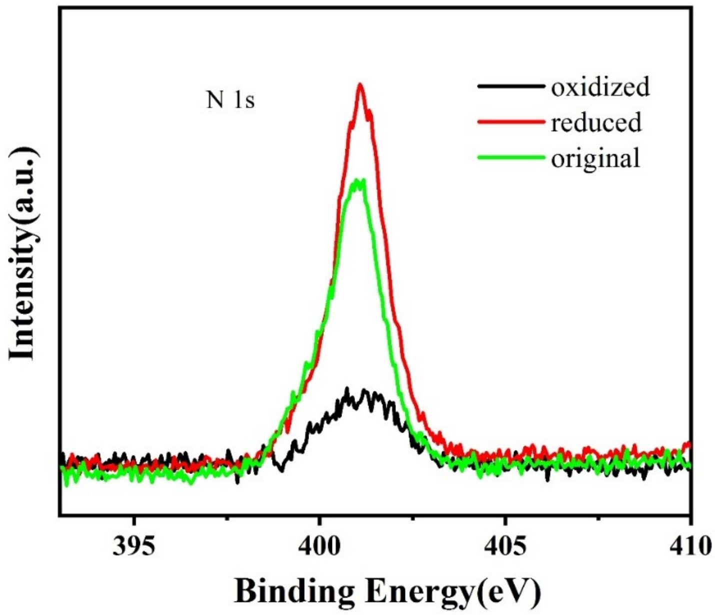

Fig. S7. The N1s of XPS pattern of electrodes at different states.

In Fig.S7, the intensity of N 1s peak for reduced electrode is higher than that of original and oxidized electrodes, indicating that lots of ammonium ions insert into the lattice of host material after the discharged process.

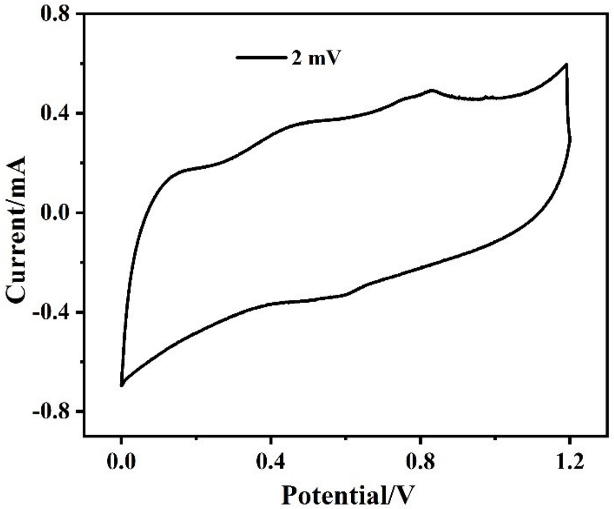

Fig. S8. The CV curve at 2 mV s^{-1} of full battery.

Fig. S8 shows the CV curve at mV s^{-1} for this aqueous ammonium ion battery based on $NH_4V_4O_{10}$ as cathode and MoS_2/MXene as anode in 0.5 mol dm^{-3} NH_4Cl electrolyte. The distinct redox peaks demonstrate that this full battery is successfully assembled.

Table S1 The performance comparison of different electrode in aqueous ammonium ion battery

Electrodes of materials	Specific capacity of cathode	Specific capacity of anode	Specific capacity of full battery	references
$Ni_2Fe(CN)_6$-R	63.4 mAh g^{-1} at 1C	—	—	[S1]
$(NH_4)_{1.47}Ni[Fe(CN)_6]_{0.88}$//PTCDI	62.6 mAh g^{-1} at 150 mA g^{-1}	158.9 mAh g^{-1} at 240 mA g^{-1}	41 mAh g^{-1} at 60 mA g^{-1}	[S2]
$FeFe(CN)_6$	76.1 mAh g^{-1} at 30 mA g^{-1}	—	—	[S3]
MnHCF//PTCDI	104 mAh g^{-1} at 100 mA g^{-1}	—	45 mAh g^{-1} at 15 mA g^{-1}	[S4]
$Na_{1.5}Ni_{1.25}Fe(CN)_6$	56.1 mAh g^{-1} at 1C	—	—	[S5]
MoO_3	115 mAh g^{-1} at 1C	—	—	[S6]
N-CuHCF	60 mAh g^{-1} at 1C	—	—	[S7]
$NH_4V_4O_{10}$-180ºC //MoS2/MXene	126.6 mAh g^{-1} at 100 mA g^{-1}	173.2 mAh g^{-1} at 100 mA g^{-1}	42 mAh g^{-1} at 100 mA g^{-1}	Our work

[S1] H. Yu, J. Xu, C. Deng, M. Xia, X. Zhang, J. Shu, Z. Wang, The Nature of the Ultrahigh Initial Coulombic Efficiency of Ni2Fe(CN)6 in Aqueous Ammonium-Ion Batteries, ACS Applied Energy Materials 4(9) (2021) 9594-9599.

[S2] X. Wu, Y. Qi, J.J. Hong, Z. Li, A.S. Hernandez, X. Ji, Rocking‐chair ammonium‐ion battery: a highly reversible aqueous energy storage system, Angewandte Chemie International Edition 56(42) (2017) 13026-13030.

[S3] S. Li, M. Xia, C. Xiao, X. Zhang, H. Yu, L. Zhang, J. Shu, Common ion effect enhanced Prussian blue analogues for aqueous ammonium ion storage, Dalton Transactions 50(19) (2021) 6520-6527.

[S4] H. Zhang, Y. Tian, W. Wang, Z. Jian, W. Chen, Organic Ammonium Ion Battery: A New Strategy for Nonmetallic Ion Energy Storage System, Angewandte Chemie (2022).

[S5] H. Yu, L. Fan, H. Yan, C. Deng, L. Yan, J. Shu, Z.-B. Wang, Nickel ferrocyanides for aqueous ammonium ion batteries, Inorganic Chemistry Frontiers 9(9) (2022) 2001-2010.

[S6] G. Liang, Y. Wang, Z. Huang, F. Mo, X. Li, Q. Yang, D. Wang, H. Li, S. Chen, C. Zhi, Initiating hexagonal MoO3 for superb‐stable and fast NH4+ storage based on hydrogen bond chemistry, Advanced Materials 32(14) (2020) 1907802.

[S7] X. Zhang, M. Xia, T. Liu, N. Peng, H. Yu, R. Zheng, L. Zhang, M. Shui, J. Shu, Copper hexacyanoferrate as ultra-high rate host for aqueous ammonium ion storage, Chemical Engineering Journal 421 (2021) 127767.